

Extraordinary Tunneling Magnetoresistance in Antiferromagnetic Tunnel Junctions with Antiperovskite Electrodes

Gautam Gurung,^{1,2*} Ding-Fu Shao,^{3,†} and Evgeny Y. Tsymbal^{1,‡}

¹ *Department of Physics and Astronomy & Nebraska Center for Materials and Nanoscience,
University of Nebraska, Lincoln, Nebraska 68588-0299, USA*

² *Trinity College, University of Oxford, Oxford OX1 3BH, UK*

³ *Key Laboratory of Materials Physics, Institute of Solid-State Physics, HFIPS, Chinese Academy of Sciences, Hefei 230031, China*

Recent theoretical predictions and experimental demonstrations of a large tunneling magnetoresistance (TMR) effect in antiferromagnetic (AFM) tunnel junctions (AFMTJs) offer a new paradigm for information technologies where the AFM Néel vector serves as a state variable. A large TMR is beneficial for the applications. Here, we predict the emergence of an extraordinary TMR (ETMR) effect in AFMTJs utilizing noncollinear AFM antiperovskite $X\text{NMn}_3$ ($X = \text{Ga}, \text{Sn}, \dots$) electrodes and a perovskite oxide ATiO_3 ($A = \text{Sr}, \text{Ba}, \dots$) barrier layer. The ETMR effect stems from the perfectly spin-polarized electronic states in the AFM antiperovskites that can efficiently tunnel through the low-decay-rate evanescent states of the perovskite oxide while preserving their spin state. Using an $\text{GaNMn}_3/\text{SrTiO}_3/\text{GaNMn}_3$ (001) AFMTJ as a representative example, we demonstrate a giant TMR ratio exceeding $10^4\%$ and originating from the ETMR effect. These results are promising for the efficient detection and control of the Néel vector in AFM spintronics.

Spintronics is a research field that exploits the spin degree of freedom for information technologies [1]. Especially promising, in this regard, are ferroic materials which allow the use of a magnetic order parameter (e.g., magnetization of a ferromagnet) as a state variable to store the information in spintronic devices. Spin-dependent transport properties of these materials are employed to distinguish the non-volatile states associated with different orientations of the magnetic order parameter. A typical example is a magnetic tunnel junction (MTJ) that consists of two ferromagnetic (FM) metal electrodes separated by a non-magnetic insulating tunneling barrier [2-6]. In MTJs, the spin-polarized tunneling current is controlled by the relative magnetization orientation of the two electrodes, known as the tunneling magnetoresistance (TMR) effect [7]. Due to TMR, MTJs can serve as building blocks of magnetic random-access memories (MRAMs) [8].

Historically, the TMR magnitude has been estimated using the empirical Julliere's formula, $\text{TMR} = \frac{2p_1p_2}{1-p_1p_2}$, where p_i ($i = 1, 2$) is the transport spin polarization of the i -th FM electrode in a MTJ [2]. Based on this formula, a larger spin polarization of the electrodes favors a larger TMR. This understanding rules out using antiferromagnetic (AFM) metals as electrodes in MTJs, due to $p_i = 0$ expected for antiferromagnets with their zero net magnetization.

Recent theoretical predictions [9-11] and experimental demonstrations [12,13] of TMR in antiferromagnetic tunnel junctions (AFMTJs) challenge this understanding. The theoretical calculations show that, in crystalline AFMTJs, TMR is determined by the momentum-dependent spin polarization of the Fermi surface of the two AFM electrodes, rather than their net spin polarizations, p_i [9-11]. TMR is then controlled by matching the spin-dependent conduction channels of the

electrodes that are determined by the AFM order parameter, known as the Néel vector. As a result, a large TMR can be obtained in AFMTJs, even in the presence of the globally spin-neutral currents [9]. The possibility of TMR in AFMTJs opens perspectives for employing antiferromagnets in MRAMs, making use of their advantages of being robust against magnetic perturbations, not producing stray fields, and exhibiting ultrafast spin dynamics [14,15].

In addition to a spin-polarized Fermi surface, the strength of TMR in AFMTJs is strongly dependent on the type of tunneling barrier. MgO is a widely used barrier material, which selectively transmits electrons from the fully spin-polarized bands of bcc-Fe(001)-based FM electrodes [16, 17], leading to a large TMR in the associated MTJs [5, 6]. While the recent experiments suggest that MgO can also be used as a tunneling barrier in AFMTJs with non-collinear AFM electrodes [12,13], this choice of the barrier material may be not optimal. This is due to the evanescent states in MgO being mostly supportive to transmission of electrons with the transverse wave vectors \mathbf{k}_\perp around the $\bar{\Gamma}$ point in the two-dimensional Brillouin zone (2DBZ) of the junction, where the spin polarization of the electrodes may be relatively small. It would be desirable to understand the effect of the tunneling barrier on TMR in AFMTJs and establish a design rule for promising electrode-barrier material combinations to realize high-performance AFMTJs.

In this letter, we predict that AFMTJs composed of non-collinear AFM antiperovskite electrodes and a perovskite oxide tunneling barrier exhibit an extraordinary TMR (ETMR) effect with a giant TMR ratio. Based on density functional theory (DFT) calculations, we demonstrate that antiperovskite GaNMn_3 , a noncollinear AFM metal, hosts conduction channels with nearly 100% effective spin polarization that match the evanescent states with low decay rates of perovskite oxide SrTiO_3 . Using GaNMn_3

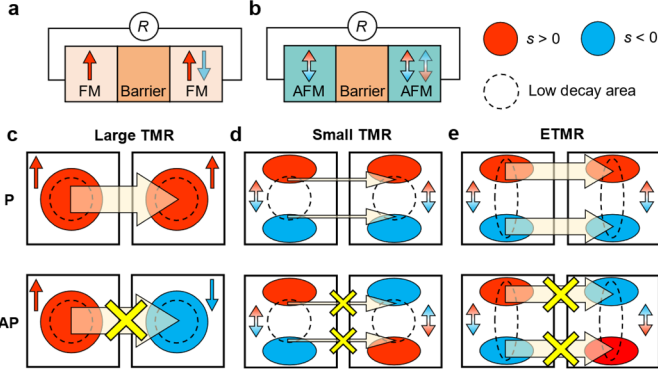


Fig. 1: (a,b) Schematics of an MTJ (a) and an AFMTJ (b). Arrows indicate magnetizations of the FM electrodes and double arrows indicate Néel vectors in the AFM electrodes. (c) A schematic TMR mechanism for an MTJ, where the fully spin-polarized conduction channels in the FM electrodes and the evanescent states with low decay rates in the barrier have an isotropic distribution in a 2DBZ around the zone center. Their matching leads to a large TMR. (d) A schematic TMR mechanism for an AFMTJ, where the AFM electrodes have the anisotropic spin-polarized conduction channels, and the barrier has an isotropic zone-centered distribution of the evanescent states with low decay rates. Their poor matching leads to a small TMR. (e) The same as (d), except the anisotropic zone-centered evanescent states with low decay rates in the barrier. Their better matching results in the ETMR effect with a large TMR ratio.

as electrodes and SrTiO_3 as a tunneling barrier, we design an $\text{GaMnN}_3/\text{SrTiO}_3/\text{GaMnN}_3$ (001) AFMTJ exhibiting the ETMR effect. Our quantum-transport calculations reveal that the perfectly spin-polarized electrons in GaMnN_3 (001) electrodes efficiently tunnel across the SrTiO_3 (001) barrier preserving their spin and leading to a giant TMR ratio exceeding 10⁴%. We argue that matching between the highly spin-polarized conduction channels in electrodes and evanescent states with low decay rates in the barrier is widely supported in antiperovskite/perovskite/antiperovskite AFMTJs and can serve as a design rule for obtaining ETMR in AFMTJs.

We start from revisiting the mechanism of TMR in an MTJ (Fig. 1(a)) and an AFMTJ (Fig. 1(b)), where the left and right electrodes are identical FM (for MTJ) or AFM (for AFMTJ) metals separated by a nonmagnetic insulating barrier layer. We assume that the tunnel junctions are fully crystalline. Then, in the transport regime conserving the transverse wave vector $\mathbf{k}_\parallel = (k_x, k_y)$ (no diffuse scattering), the tunneling conductance per a transverse unit cell area is given by

$$G = \frac{e^2}{h} \frac{1}{(2\pi)^2} \int T(\mathbf{k}_\parallel) d\mathbf{k}_\parallel, \quad (1)$$

where $T(\mathbf{k}_\parallel)$ is spin-dependent transmission between left and right metal electrodes at \mathbf{k}_\parallel . A large $T(\mathbf{k}_\parallel)$ requires three conditions: (1) conduction channels must be available in the two

electrodes at wave vector \mathbf{k}_\parallel ; (2) decay rate $\kappa_{\mathbf{k}_\parallel}$ of the evanescent state at \mathbf{k}_\parallel in the tunneling barrier must be low; and (3) spin states of the conduction channels at \mathbf{k}_\parallel in the two electrodes should be matched. Condition (1) is necessary for having $T(\mathbf{k}_\parallel) \neq 0$. Condition (2) is required to support reduced attenuation of the transmitted wave in the barrier. Condition (3) provides matching of the spin components of the wave functions in the electrodes supporting transmission.

The spin state can be quantified in terms of the net spin $\mathbf{s}_{\mathbf{k}_\parallel}$ of the conduction channels available in electrodes at the transverse wave vector \mathbf{k}_\parallel :

$$\mathbf{s}_{\mathbf{k}_\parallel} = \sum_n \mathbf{s}_{\mathbf{k}_\parallel n} = \sum_n \frac{l_z}{2\pi} \int \langle n\mathbf{k} | \mathbf{s} | n\mathbf{k} \rangle \delta(E_{n\mathbf{k}} - E_F) dk_z. \quad (2)$$

Here l_z is the lattice constant of the electrode along the transport direction, $\langle n\mathbf{k} | \mathbf{s} | n\mathbf{k} \rangle$ is the spin expectation value for band n of energy $E_{n\mathbf{k}}$ at wave vector $\mathbf{k} = (\mathbf{k}_\parallel, k_z)$, and E_F is the Fermi energy.

For collinear magnets, $\mathbf{s}_{\mathbf{k}_\parallel}$ is collinear to the magnetic order parameter, and its magnitude, $s_{\mathbf{k}_\parallel} = N_{\mathbf{k}_\parallel}^\uparrow - N_{\mathbf{k}_\parallel}^\downarrow$, is determined by the number of conduction channels $N_{\mathbf{k}_\parallel}^{\uparrow,\downarrow}$ for up- (\uparrow) and down- (\downarrow) spin electrons at \mathbf{k}_\parallel . In this case, the net spin controls the spin polarization of conduction channels in the electrodes given by

$p_{\mathbf{k}_\parallel} = \frac{s_{\mathbf{k}_\parallel}}{\sum_n |s_{\mathbf{k}_\parallel n}|} = \frac{N_{\mathbf{k}_\parallel}^\uparrow - N_{\mathbf{k}_\parallel}^\downarrow}{N_{\mathbf{k}_\parallel}}$, where $N_{\mathbf{k}_\parallel}$ is the total number of conduction channels at \mathbf{k}_\parallel [9]. Due to spin being conserved in the tunneling process, transmission $T(\mathbf{k}_\parallel)$ is controlled by condition (3). For example, for an MTJ with parallel magnetization of the electrodes (P state, Fig. 1(c) top), $T(\mathbf{k}_\parallel)$ is large and strongly spin polarized in a wide area of the 2DBZ. On the contrary, for antiparallel magnetization (AP state, Fig. 1(c) bottom), condition (3) is not satisfied, and $T(\mathbf{k}_\parallel)$ is suppressed. As a result, the total transmission for the P state (T_P) is much larger than that for the AP state (T_{AP}), leading to a large TMR ratio, $(T_P - T_{AP})/T_{AP}$. This situation occurs, e.g., in Fe/MgO/Fe (001) MTJs [16,17], where Fe (001) electrodes have highly spin-polarized conduction channels around the 2DBZ center (large $p_{\mathbf{k}_\parallel}$), matching the lowest decay rate of MgO and thus resulting in a large TMR.

For noncollinear magnets, spin is not a good quantum number and, in general, is not conserved in the tunneling process. Nevertheless, we can define the *effective* spin polarization $\mathbf{p}_{\mathbf{k}_\parallel} = \frac{\mathbf{s}_{\mathbf{k}_\parallel}}{\sum_n |s_{\mathbf{k}_\parallel n}|}$ as a vector that has different magnitudes and orientations at different \mathbf{k}_\parallel . As seen from the definition, the magnitude of the spin polarization $p_{\mathbf{k}_\parallel} = |\mathbf{p}_{\mathbf{k}_\parallel}|$ is equal to 100% when spins $\mathbf{s}_{\mathbf{k}_\parallel n}$ are parallel in all conduction channels n at \mathbf{k}_\parallel or when only one conduction channel is present. This situation is reminiscent to the collinear magnet case, where spin is conserved in the process of

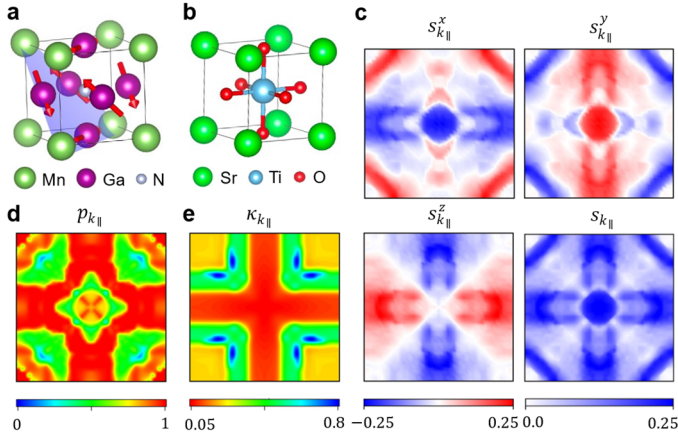


Fig. 2: (a) The atomic and magnetic structure of antiperovskite GaNMn₃ in the noncollinear Γ_{5g} AFM configuration. (b) The atomic structure of perovskite SrTiO₃. (c) Components of the net spin $\mathbf{s}_{\mathbf{k}_{||}} = (s_{\mathbf{k}_{||}}^x, s_{\mathbf{k}_{||}}^y, s_{\mathbf{k}_{||}}^z)$ and $s_{\mathbf{k}_{||}} \equiv |\mathbf{s}_{\mathbf{k}_{||}}|$ in the 2DBZ of GaNMn₃ (001). (d) The magnitude of the effective spin polarization $p_{\mathbf{k}_{||}} = |\mathbf{p}_{\mathbf{k}_{||}}|$ in the 2DBZ of GaNMn₃ (001). (e) The lowest decay rate $\kappa_{\mathbf{k}_{||}}$ of the evanescent states of SrTiO₃ (001) in the 2DBZ calculated at the energy close to the bottom of the conduction band.

tunneling. As a result, matching of the net spins $\mathbf{s}_{\mathbf{k}_{||}}$ in the electrodes can be used as requirement (3) for large transmission $T(\mathbf{k}_{||})$ in the areas of the 2DBZ where $p_{\mathbf{k}_{||}}$ is close to 100%. The latter condition can then be used for determining the regions in the 2DBZ where the spin is virtually conserved. We note that the effective spin polarization is $\mathbf{k}_{||}$ -dependent and thus is different from the conventional spin polarization which is defined with respect to a global spin quantization axis. Also, at those $\mathbf{k}_{||}$ where there are a few conduction channels with non-collinear $\mathbf{s}_{\mathbf{k}_{||}}$, spin is not conserved in the tunneling process and thus $p_{\mathbf{k}_{||}}$ could not serve as a proper measure of TMR in the spirit of Julliere's formula.

In order to have non-vanishing TMR in AFMTJs, AFM electrodes with broken $\hat{P}\hat{T}$ and $\hat{U}\hat{t}$ symmetries are required, where \hat{P} is inversion symmetry, \hat{T} is time reversal symmetry, \hat{U} is spin rotation symmetry, and \hat{t} is half a unit cell translation. In these antiferromagnets, Kramers' degeneracy of their electronic bands is broken even in the absence of spin-orbit coupling. As a result, the spin-split Fermi surfaces hold conduction channels with finite $\mathbf{s}_{\mathbf{k}_{||}}$ (and thus spin polarization $\mathbf{p}_{\mathbf{k}_{||}}$) as has been demonstrated both for collinear [9] and for noncollinear antiferromagnets [11,18]. Normally, the magnetization of these antiferromagnets is compensated by certain crystal symmetries such as mirror planes and/or rotation axes. Often, these symmetries lead to an anisotropic distribution of $\mathbf{s}_{\mathbf{k}_{||}}$ in the 2DBZ with the magnitude $s_{\mathbf{k}_{||}}$ being small along the symmetry invariant lines (planes). For example, mirror plane \hat{M}_y perpendicular to the y axis leads to a symmetric distribution of

$s_{\mathbf{k}_{||}}^y$ and an antisymmetric distribution of $s_{\mathbf{k}_{||}}^x$ and $s_{\mathbf{k}_{||}}^z$ with respect to the mirror invariant line $k_y = 0$, resulting in $s_{\mathbf{k}_{||}}^x = s_{\mathbf{k}_{||}}^z = 0$ along this line. Therefore, in an AFMTJ composed of such AFM electrodes, there is a mismatch between the anisotropic high- $\mathbf{p}_{\mathbf{k}_{||}}$ area in the electrodes and the nearly isotropic zone-centered low- $\kappa_{\mathbf{k}_{||}}$ area in the barrier resulting a relatively small TMR (Fig. 1(d)). For a high-performance AFMTJ, it would be desirable to have a barrier with an anisotropic low- $\kappa_{\mathbf{k}_{||}}$ area matching the high- $\mathbf{p}_{\mathbf{k}_{||}}$ conduction channels in the electrodes and thus producing the ETMR effect (Fig. 1(e)).

This matching can be realized in AFMTJs composed of XNMn₃-type ($X = \text{Ga, Sn, ...}$) antiperovskite electrodes and an ATiO₃-type ($A = \text{Sr, Ba, ...}$) perovskite barrier. Antiperovskites have cubic structures similar to perovskites, except the positions of anions and cations being interchanged (Fig. 2(a,b)). The frustrated Mn-kagome lattice in the (111) plane favors the noncollinear AFM configurations, resulting in interesting physical properties, such as magnetovolume [19], barocaloric [20], piezomagnetic [21,22,23], magnetoelectric [24, 25], and anomalous Hall [26-30] effects and unconventional spin currents [18, 31, 32].

Figure 2(a) shows the atomic and magnetic structure of GaNMn₃ – a representative noncollinear AFM antiperovskite, where Mn magnetic moments form a 120° chiral configuration within the (111) plane. Such a Γ_{5g} noncollinear AFM structure breaks $\hat{P}\hat{T}$ and $\hat{U}\hat{t}$ symmetries, resulting in a spin-polarized Fermi surface (Fig. S1) and hence spin-polarized conduction channels. Figure 2(c) shows the calculated components of the net spin $\mathbf{s}_{\mathbf{k}_{||}} = (s_{\mathbf{k}_{||}}^x, s_{\mathbf{k}_{||}}^y, s_{\mathbf{k}_{||}}^z)$ in the 2DBZ of GaNMn₃ (001) (see also Fig. S2). Due to a mirror plane $\hat{M}_{\bar{1}10}$ and a two-fold rotation axis $\hat{C}_{\bar{1}10}$, $s_{\mathbf{k}_{||}}^z$ vanishes along the diagonals parallel to k_{110} and $k_{\bar{1}10}$ in the 2DBZ. This follows from the symmetry transformations of wave vector \mathbf{k} and spin \mathbf{s} :

$$\begin{aligned}\hat{M}_{\bar{1}10}(k_{110}, k_{\bar{1}10}, k_{001}) &= (k_{110}, -k_{\bar{1}10}, k_{001}), \\ \hat{C}_{\bar{1}10}(k_{110}, k_{\bar{1}10}, k_{001}) &= (-k_{110}, k_{\bar{1}10}, -k_{001}), \\ \hat{M}_{\bar{1}10}(\langle s_{110} \rangle, \langle s_{\bar{1}10} \rangle, \langle s_{001} \rangle) &= (-\langle s_{110} \rangle, \langle s_{\bar{1}10} \rangle, \langle s_{001} \rangle), \\ \hat{C}_{\bar{1}10}(\langle s_{110} \rangle, \langle s_{\bar{1}10} \rangle, \langle s_{001} \rangle) &= (\langle s_{110} \rangle, -\langle s_{\bar{1}10} \rangle, -\langle s_{001} \rangle).\end{aligned}$$

As a result, $s_{\mathbf{k}_{||}}$ is relatively small for the conduction channels along the diagonals of the 2DBZ, so that the largest $s_{\mathbf{k}_{||}}$ appears at $k_x = 0$ and $k_y = 0$, forming a cross pattern of $s_{\mathbf{k}_{||}} \equiv |\mathbf{s}_{\mathbf{k}_{||}}|$ in Fig. 2(c) (right bottom panel). It is notable that the spin polarization distribution has a similar cross feature in the 2DBZ with $p_{\mathbf{k}_{||}}$ values close to 100% (Fig. 2(d)) – an unexpected feature for noncollinear antiferromagnets. This distribution of $p_{\mathbf{k}_{||}}$ is reminiscent to the shape of the lowest decay rate $\kappa_{\mathbf{k}_{||}}$ of the evanescent states in perovskite SrTiO₃ [33, 34]. Figure 2(e)

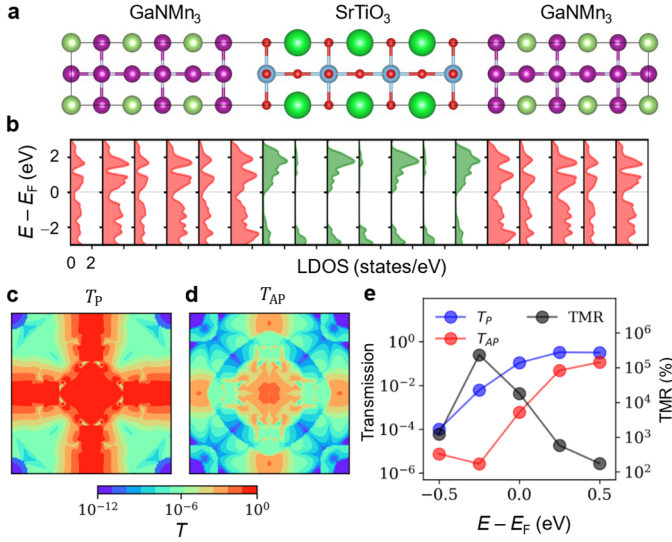


Fig. 3: (a,b) The atomic structure (a) and layer-resolved density of states (LDOS) (b) of GaNMn₃/SrTiO₃/GaNm₃ (001) AFMTJ. (c,d) The calculated k_{\parallel} -resolved transmission in the 2DBZ for the AFMTJ for P (c) and AP (d) alignment of the Néel vector in GaNMn₃ electrodes. (e) Total transmission and TMR as functions of energy.

shows that $\kappa_{k_{\parallel}}$ has an analogous cross pattern feature in the 2DBZ. Such matching between the high- $p_{k_{\parallel}}$ and low- $\kappa_{k_{\parallel}}$ areas in the 2DBZ suggests that GaNMn₃ and SrTiO₃ are a promising material combination for the AFM electrode and the tunneling barrier for an AFMTJ where the ETMR can be observed.

Following this argument, we assemble an GaNMn₃/SrTiO₃/GaNm₃ (001) AFMTJ. Due to the similar atomic structures and lattice constants, such a high-quality crystalline AFMTJ is feasible in practice. In fact, epitaxial GaNMn₃ films have been grown on SrTiO₃ revealing high crystallinity of their interface structure [35]. Figure 3(a) shows the atomic structure of the AFMTJ that is used in our calculations. Here a 3-unit-cell SrTiO₃ (001) barrier layer is placed between 2.5-unit-cell GaNMn₃ layers. The layers are connected at the Mn₂N/TiO₂ interfaces which have the lowest energy among other interfaces considered [25]. We find that a wide band gap of SrTiO₃ is well maintained across the junction (Fig. 3(b)). The GaNMn₃/SrTiO₃/GaNm₃ (001) structure in Fig. 3(a) is then used as the scattering region of the AFMTJ connected to two semi-infinite GaNMn₃ (001) electrodes for transmission calculation [36].

For the P state, where the Néel vectors of the two electrodes are parallel, $T_P(k_{\parallel})$ is strongly enhanced in a cross-pattern area of the 2DBZ, resulting from the high- $p_{k_{\parallel}}$ -low- $\kappa_{k_{\parallel}}$ matching in this area. In contrast, for the AP state, where the Néel vectors of the two electrodes are antiparallel, while the largest $T_{AP}(k_{\parallel})$ also appears at the cross-pattern area, it is significantly reduced compared to $T_P(k_{\parallel})$ due to reversed $s_{k_{\parallel}}$ in the two electrodes. As a result, the total transmission T_{AP} is much smaller than T_P ,

producing the TMR ratio $(T_P - T_{AP})/T_{AP}$ as large as $\sim 1.8 \times 10^4\%$ (Fig. 3(e)). This TMR value is gigantic, significantly larger than the values known for conventional MTJs and reminiscent to an infinitely large TMR expected for MTJs based on ideal half-metallic electrodes. This extraordinary behavior of the GaNMn₃/SrTiO₃/GaNm₃ (001) AFMTJ is due to the remarkable property of antiperovskite GaNMn₃ to exhibit fully spin-polarized electronic states that can efficiently tunnel through perovskite SrTiO₃ while preserving their spin state – the signature of the ETMR effect.

We note that in our calculation, the Fermi energy (E_F) of the AFMTJ lies near the conduction band minimum (CBM) of SrTiO₃ (Fig. 3 (b)), while it is expected to appear well within the band gap of the insulator. This is due to the underestimated band gap of SrTiO₃ resulting from the well-known deficiency of DFT to correctly describe the excited states. Such a shortage, however, does not affect our main conclusions, since the giant TMR appears not only for $E = E_F$ but also in a broad energy window around E_F (Fig. 3(e)). Especially, we obtain an even larger ETMR of $\sim 2.3 \times 10^5\%$ at $E = E_F - 0.25$ eV, well inside the band gap of SrTiO₃, indicating the validity of our results. In addition, we find that the cross feature of the evanescent states persists much deeper in the band gap of SrTiO₃ (Fig. S4), suggesting that independent of the band offset between GaNMn₃ and SrTiO₃, matching between the highly polarized conducting channels in GaNMn₃ and low decay rate evanescent states in SrTiO₃ is well maintained. Note that ETMR is reduced for energies above the CBM of SrTiO₃, which is expected since the SrTiO₃ becomes conducting (Fig. 3(e)).

In addition to the AFM Γ_{5g} phase, there is another common noncollinear AFM configuration of antiperovskites known as the Γ_{4g} phase [37-39]. The AFM Γ_{4g} phase is obtained from Γ_{5g} by rotating all magnetic moments about the [111] axis by 90°. The corresponding distribution of $s_{k_{\parallel}}$ in GaNMn₃ in the AFM Γ_{4g} state mirrors this rotation (Fig. S5(a,b), top panels). This spin rotation, however, does not change the patterns of $s_{k_{\parallel}}$ and $p_{k_{\parallel}}$ (Fig. S5(a,b), middle and bottom panels) which remain the same as those for the Γ_{5g} phase. Therefore, the giant ETMR is also expected for GaNMn₃/SrTiO₃/GaNm₃ (001) AFMTJs with GaNMn₃ electrodes in the AFM Γ_{4g} phase.

Apart from GaNMn₃, other AFM antiperovskites can be used as electrodes in AFMTJs. For example, SnNMn₃ – a high-temperature noncollinear antiferromagnet [32,37], also has a sizable spin $s_{k_{\parallel}}$ along the $k_x = 0$ and $k_y = 0$ lines in the 2DBZ and a very large spin polarization $p_{k_{\parallel}}$ over a substantial part of the 2DBZ for both Γ_{4g} and Γ_{5g} phases (Fig. S5(c,d)). These properties indicate a possibility of the ETMR effect in SnNMn₃/SrTiO₃/SnNMn₃ AFMTJs. In addition, other perovskite oxides, such as BaTiO₃, host a low- $\kappa_{k_{\parallel}}$ cross area [40], and hence can be used as a barrier in antiperovskite/perovskite/antiperovskite AFMTJs. Particularly attractive is

making use of ferroelectricity of BaTiO₃ to design a multiferroic tunnel junction where the ETMR and TER (tunneling electroresistance [41]) effects coexist. Finally, the giant ETMR indicates a possibility of a strong spin-transfer torque in these AFMTJs [42,43], which may offer an efficient electrical method for ultrafast switching of the Néel vector.

In conclusion, we have predicted the ETMR effect in AFMTJs composed of non-collinear AFM antiperovskite electrodes and a perovskite oxide tunnel barrier. The origin of ETMR stems from the perfectly spin-polarized electronic states in the AFM antiperovskites that can efficiently tunnel through the perovskite oxide barrier while preserving their spin state. Our quantum-transport calculations reveal a giant TMR ratio $\sim 10^4\%$ for GaMn₃/SrTiO₃/GaMn₃ (001) AFMTJs, originating from matching the highly spin-polarized conduction channels in AFM antiperovskite GaMn₃ and the low-decay-rate evanescent states in perovskite SrTiO₃. The predicted ETMR effect is expected to be widely supported in other antiperovskite/perovskite/antiperovskite AFMTJs. Our results are promising for

the efficient detection and control of the Néel vector in AFM spintronics, and thus we encourage experimentalists working in this field to verify our predictions.

Acknowledgments. The authors thank Dr. Bimal Neupane of University of North Texas for his help in calculations. This work was supported by the Office of Naval Research (ONR grant N00014-20-1-2844) (G.G., E.Y.T). G.G. gratefully acknowledges support of a Junior Research Fellowship from Trinity College, Oxford, U.K. D.F.S. acknowledges support from the National Key Research and Development Program of China (Grant Nos. 2021YFA1600200) and the National Science Foundation of China (NSFC Grants No. 12241405, 12274411). Computations were performed at the University of Nebraska Holland Computing Center.

* gautam.gurung@trinity.ox.ac.uk

† dfshao@issp.ac.cn

‡ tsymbal@unl.edu

- [1] E. Y. Tsymlal and I. Žutić, Eds., *Spintronics Handbook: Spin Transport and Magnetism*, 2-nd edition (CRC press, 2019).
- [2] M. Julliere, Tunneling between ferromagnetic films, *Phys. Lett. A* **54**, 225 (1975).
- [3] R. Meservey and P. M. Tedrow, Spin-polarized electron tunneling, *Phys. Rep.* **238**, 173 (1994).
- [4] J. S. Moodera, L. R. Kinder, T. M. Wong, and R. Meservey, Large magnetoresistance at room temperature in ferromagnetic thin film tunnel junctions, *Phys. Rev. Lett.* **74**, 3273 (1995).
- [5] S. Yuasa, T. Nagahama, A. Fukushima, Y. Suzuki, and K. Ando, Giant room-temperature magnetoresistance in single-crystal Fe/MgO/Fe magnetic tunnel junctions, *Nat. Mater.* **3**, 868 (2004).
- [6] S. Parkin, C. Kaiser, A. Panchula, P. M. Rice, B. Hughes, M. Samant, and S. H. Yang, Giant tunnelling magnetoresistance at room temperature with MgO (100) tunnel barriers, *Nat. Mater.* **3**, 862 (2004).
- [7] E. Y. Tsymlal, O. N. Mryasov, and P. R. LeClair, Spin-dependent tunneling in magnetic tunnel junctions, *J. Phys.: Condens. Matter* **15**, R109 (2003).
- [8] A. V. Khvalkovskiy, D. Apalkov, S. Watts, R. Chepulskii, R. S. Beach, A. Ong, X. Tang, A. Driskill-Smith, W. H. Butler, P. B. Vischer, D. Lottis, E. Chen, V. Nikitin, and M. Krounbi, Basic principles of STT-MRAM cell operation in memory arrays, *J. Phys. D* **46**, 074001 (2013).
- [9] D.-F. Shao, S. H. Zhang, M. Li, C. B. Eom, and E. Y. Tsymlal, Spin-neutral currents for spintronics, *Nat. Commun.* **12**, 7061 (2021).
- [10] L. Šmejkal, A. Birk Hellenes, R. González-Hernández, J. Sinova, and T. Jungwirth, Giant and tunneling magnetoresistance in unconventional collinear antiferromagnets with nonrelativistic spin-momentum coupling, *Phys. Rev. X* **12**, 011028 (2022).
- [11] J. Dong, X. Li, G. Gurung, M. Zhu, P. Zhang, F. Zheng, E. Y. Tsymlal, and J. Zhang, Tunneling magnetoresistance in noncollinear antiferromagnetic tunnel junctions, *Phys. Rev. Lett.* **128**, 197201 (2022).
- [12] P. Qin, H. Yan, X. Wang, H. Chen, Z. Meng, J. Dong, M. Zhu, J. Cai, Z. Feng, X. Zhou, L. Liu, T. Zhang, Z. Zeng, J. Zhang, C. Jiang, and Z. Liu, Room-temperature magnetoresistance in an all-antiferromagnetic tunnel junction, *Nature* **613**, 485 (2023).
- [13] X. Chen, T. Higo, K. Tanaka, T. Nomoto, H. Tsai, H. Idzuchi, M. Shiga, S. Sakamoto, R. Ando, H. Kosaki, T. Matsuo, D. Nishio-Hamane, R. Arita, S. Miwa, and S. Nakatsuji, Octupole-driven magnetoresistance in an antiferromagnetic tunnel junction, *Nature* **613**, 490 (2023).
- [14] V. Baltz, A. Manchon, M. Tsoi, T. Moriyama, T. Ono, and Y. Tserkovnyak, Antiferromagnetic spintronics, *Rev. Mod. Phys.* **90**, 015005 (2018).
- [15] T. Jungwirth, X. Marti, P. Wadley, and J. Wunderlich, Antiferromagnetic spintronics, *Nat. Nanotechnol.* **11**, 231 (2016).
- [16] W. H. Butler, X.-G. Zhang, T. C. Schulthess, and J. M. MacLaren, Spin-dependent tunneling conductance of Fe|MgO|Fe sandwiches, *Phys. Rev. B* **63**, 054416 (2001).
- [17] J. Mathon and A. Umerski, Theory of tunneling magnetoresistance of an epitaxial Fe/MgO/Fe(001) junction, *Phys. Rev. B* **63**, 220403(R) (2001).
- [18] G. Gurung, D. F. Shao, E. Y. Tsymlal, Transport spin polarization of noncollinear antiferromagnetic antiperovskites, *Phys. Rev. Mater.* **5**, 124411 (2021).
- [19] K. Takenaka, M. Ichigo, T. Hamada, A. Ozawa, T. Shibayama, T. Inagaki, and K. Asano, Magnetovolume effects in manganese nitrides with antiperovskite structure. *Sci. Tech. Adv. Mat.* **15**, 015009 (2014).
- [20] D. Matsunami, A. Fujita, K. Takenaka, and M. Kano, Giant barocaloric effect enhanced by the frustration of the antiferromagnetic phase in Mn₃GaN. *Nat. Mater.* **14**, 73 (2015).
- [21] P. Lukashev, R. F. Sabirianov, and K. Belashchenko, Theory of piezomagnetic effect in Mn-based antiperovskites, *Phys. Rev. B* **78**, 184414 (2008).
- [22] J. Zemen, Z. Gercsi, and K. G. Sandeman, Piezomagnetism as a counterpart of the magnetovolume effect in magnetically frustrated Mn-based antiperovskite nitrides, *Phys. Rev. B* **96**, 024451 (2017).

- [23] D. Boldrin, A. P. Mihai, B. Zou, J. Zemen, R. Thompson, E. Ware, B. V. Neamtu, L. Ghivelder, B. Esser, D. W. McComb, P. Petrov, and L. F. Cohen, Giant piezomagnetism in Mn_3NiN , *ACS Appl. Mater. & Int.* **10**, 18863 (2018).
- [24] P. Lukashev, K. D. Belashchenko, and R. F. Sabirianov, Large magnetoelectric effect in ferroelectric/piezomagnetic heterostructures, *Phys. Rev. B* **84**, 133420 (2011).
- [25] D. F. Shao, G. Gurung, T. R. Paudel, and E. Y. Tsymbal, Electrically reversible magnetization at the antiperovskite/perovskite interface, *Phys. Rev. Mater.* **3**, 024405 (2019).
- [26] G. Gurung, D.-F. Shao, T. R. Paudel, and E. Y. Tsymbal, Anomalous Hall conductivity of non-collinear magnetic antiperovskites, *Phys. Rev. Mater.* **3**, 044409 (2019).
- [27] D. Boldrin, I. Samathrakos, J. Zemen, A. Mihai, B. Zou, B. Esser, D. McComb, P. Petrov, H. Zhang, and L. F. Cohen, The anomalous Hall effect in non-collinear antiferromagnetic Mn_3NiN thin films, *Phys. Rev. Mater.* **3**, 094409 (2019).
- [28] X. Zhou, J.-P. Hanke, W. Feng, F. Li, G.-Y. Guo, Y. Yao, S. Blügel, and Y. Mokrousov, Spin-order dependent anomalous Hall effect and magneto-optical effect in the noncollinear antiferromagnets Mn_3XN with $X = \text{Ga}, \text{Zn}, \text{Ag}, \text{or Ni}$, *Phys. Rev. B* **99**, 104428 (2019).
- [29] K. Zhao, T. Hajiri, H. Chen, R. Miki, H. Asano, and P. Gegenwart, Anomalous Hall effect in the noncollinear antiferromagnetic antiperovskite $\text{Mn}_3\text{Ni}_{1-x}\text{Cu}_x\text{N}$, *Phys. Rev. B* **100**, 045109 (2019).
- [30] Y. You, H. Bai, X. Chen, Y. Zhou, X. Zhou, F. Pan, and C. Song, Room temperature anomalous Hall effect in antiferromagnetic Mn_3SnN films, *Appl. Phys. Lett.* **117**, 222404 (2020).
- [31] T. Nan, C. X. Quintela, J. Irwin, G. Gurung, D. F. Shao, J. Gibbons, N. Campbell, K. Song, S. Y. Choi, L. Guo, R. D. Johnson, P. Manuel, R. V. Chopdekar, I. Hallsteinsen, T. Tybell, P. J. Ryan, J. W. Kim, Y. S. Choi, P. G. Radaelli, D. C. Ralph, E. Y. Tsymbal, M. S. Rzchowski, and C. B. Eom, Controlling spin current polarization through non-collinear antiferromagnetism, *Nat. Commun.* **11**, 4671 (2020).
- [32] Y. You, H. Bai, X. Feng, X. Fan, L. Han, X. Zhou, Y. Zhou, R. Zhang, T. Chen, F. Pan, and C. Song, Cluster magnetic octupole induced out-of-plane spin polarization in antiperovskite antiferromagnet, *Nat. Commun.* **12**, 6524 (2021).
- [33] J. P. Velev, K. D. Belashchenko, D. A. Stewart, M. van Schilfgaarde, S. S. Jaswal, and E. Y. Tsymbal, Negative spin polarization and large tunneling magnetoresistance in epitaxial $\text{Co}[\text{SrTiO}_3]\text{Co}$ magnetic tunnel junctions. *Phys. Rev. Lett.* **95**, 216601 (2005).
- [34] K. Janicka, J. P. Velev, and E. Y. Tsymbal, Quantum nature of two-dimensional electron gas confinement at $\text{LaAlO}_3/\text{SrTiO}_3$ interfaces, *Phys. Rev. Lett.* **102**, 106803 (2009).
- [35] C. X. Quintela, K. Song, D.-F. Shao, L. Xie, T. Nan, T. R. Paudel, N. Campbell, X. Pan, T. Tybell, M. S. Rzchowski, E. Y. Tsymbal, S.-Y. Choi, and C.-B. Eom, Epitaxial antiperovskite/perovskite heterostructures for materials design, *Sci. Adv.* **6**, eaba4017 (2020).
- [36] See Supplementary Material for the details of DFT calculations of the electronic structure and transmission, the spin textured Fermi surface and the spin-resolved band structure of GaNMn_3 , the complex band structure of SrTiO_3 , the spin texture of GaNMn_3 and SnNMn_3 in noncollinear AFM Γ_{5g} and Γ_{4g} phases, and the spin-resolved Fermi surface and band structure of SnNMn_3 .
- [37] D. Fruchart and E. F. Bertaut, Magnetic studies of the metallic perovskite-type compounds of manganese. *J. Phys. Soc. Jap.* **44**, 781 (1978).
- [38] K. Takenaka, T. Inagaki, and H. Takagi, Conversion of magnetic structure by slight dopants in geometrically frustrated antiperovskite Mn_3GaN . *Appl. Phys. Lett.* **95**, 132508 (2009).
- [39] Y. Wang, H. Zhang, J. Zhu, X. Liu, S. Li, R. Zou, and Y. Zhao, Antiperovskites with exceptional functionalities. *Adv. Mater.* **32**, 1905007 (2020).
- [40] J. P. Velev, C. G. Duan, K. D. Belashchenko, S. S. Jaswal, and E. Y. Tsymbal, Effect of ferroelectricity on electron transport in $\text{Pt}/\text{BaTiO}_3/\text{Pt}$ tunnel junctions, *Phys. Rev. Lett.* **98**, 137201 (2007).
- [41] J. P. Velev, J. D. Burton, M. Y. Zhuravlev, and E. Y. Tsymbal, Predictive modelling of ferroelectric tunnel junctions, *npj Comp. Mater.* **2**, 16009 (2016).
- [42] S. Ghosh, A. Manchon, and J. Železný, Unconventional Robust Spin-Transfer Torque in Noncollinear Antiferromagnetic Junctions, *Phys. Rev. Lett.* **128**, 097702 (2022).
- [43] D.-F. Shao, Y.-Y. Jiang, J. Ding, S.-H. Zhang, Z.-A. Wang, R.-C. Xiao, G. Gurung, W. J. Lu, Y. P. Sun, and E. Y. Tsymbal, Néel spin currents in antiferromagnets, *Phys. Rev. Lett.* **130**, 216702 (2023).